ISSN No: 2348-4845
International Journal & Magazine of Engineering, Technology, Management and Research
A Peer Reviewed Open Access International Journal

Effect of Reynolds Number and Wall Temperature on Shock Wave / Boundary Layer Interaction

B.Nagaraj
Assistant Professor,
Dept. of Aeronautical Engineering MLRIT,
Hyderbad.

MD.Zakiuddin
M.Tech Student
Dept. of Aeronautical Engineering MLRIT,
Hyderbad.

Abstract

At high Mach flows shock waves generated at different parts of vehicle interact withboundary layer over the surface. The adverse pressure gradient across strong shock wave causes the flow to separate. At separation point and reattachment points peak loads are generated. In this report canonical geometry of compression corner is taken to study the effect of Reynolds number and wall temperature on separation bubble size using CFD tool with Fluent package. Reynolds-averaged Navier-Stokes equations using one-equation Spalart-Allmaras turbulence model is used in simulations for flow over compression corner configuration with deflection angle of 28 degrees with Mach of 4.95. Finite volume formulation is used to discretize the governing equations using Roe scheme. Gauss Siedal iteration method is used to obtain steady state solution.In the first stage of work, inviscid simulation was carried out and compared with analytical values. In the second stage, Reynolds number is varied and its effect on separation bubble size is studied. Lastly, the wall temperature is varied and the effect of wall cooling and wall heating on separation bubble size is studied.

Keywords: ***shock wave, turbulent boundary layer, separation bubble, hypersonic***

Introduction

The interaction of shock waves with boundary layers is a basic fluid-dynamics phenomenon that has both fundamental and practical importance. The subject of shock wave boundary layer interaction continues to be an important area of research in view of its many application in both external and internal aerodynamics. Shock wave boundary layer interactions occur on air foils and in turbo-machinery blades in transonic flow, in supersonic intakes, and ahead of control surfaces, often associated with these and flares in supersonic, to cite just a few of the application,. Flow separation, often associated with these interactions,generally leads to increased energy losses in the system and degrades the performance of the aerodynamic device; flow unsteadiness, often a result of separation, can cause additional problem which are undesirable in practice. Effect of Reynolds Number and wall temperature on Separation, is beneficial for improving the design of the device under consideration.

From the engineering viewpoint, this problem can have a significant influence on aircraft or rocket performance and often leads to extremely undesirable effects, such as drag rise, massive flow separation, shock unsteadiness and high wall heating. From the fundamental point of view, this phenomenon represents one of the simplest flow configurations yielding a strong viscous/ inviscid interaction, and is therefore an ideal test case for Navier-Stokes solvers. In this problem, several viscous phenomena are observed,including a boundary layer with adverse pressure gradients, induced separation, shear layers, and a recirculation bubble. Previous studies on supersonic bounded flows have shown that shock-wave/boundary-layer interactions occurring in many situations, such as ducts, wind tunnels, nozzles or ramps, may exhibit strong unsteadiness that causes large shock excursions associated with amplified wall-pressure fluctuations.

At high Reynolds number, the boundary layers on the vehicle surface is often turbulent. The turbulent

ISSN No: 2348-4845
International Journal & Magazine of Engineering, Technology, Management and Research
A Peer Reviewed Open Access International Journal

fluctuations in a boundary layer get amplified on passing through a shock wave. The interaction of turbulent fluctuations with a shock wave involves complex physical processes, which determine the magnitude of turbulent fluctuations downstream of the shock. The level of turbulence amplification at the shock has a significant effect on the shock/boundary layer interaction, specifically on the extent of flow separation and the peak heating at reattachment.

Reynolds-averaged Navier-Stokes (RANS) methods are usually employed to simulate such flows, where the effect of turbulent fluctuations on the mean flow field is accounted by using turbulence models. Most of the conventional turbulence models are developed in low-speed flows and they cannot reproduce the complex physical effects involved in shock/turbulence interaction. This puts severe limitation on the accuracy of the computed flow solution in the presence of strong shock waves. The separation bubble size is often predicted incorrectly, and it results in a flow topology that does not match experimental observations.

The turbulent fluctuations in a flow are inherently unsteady and their interaction with the shock is also an unsteady process. RANS methods are based on time-averaged equations and therefore cannot account for this unsteady interaction between the turbulent fluctuations and the shock wave. This has been pointed out as one of the major limitations of existing turbulence models were the first to study the effect of unsteady shock motion in the RANS framework.

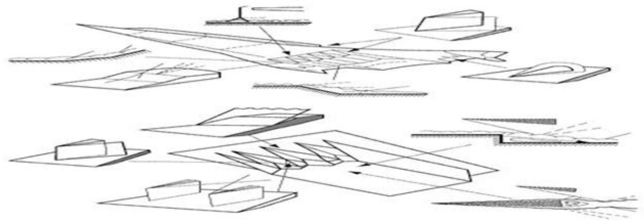

Figure 1.1: Example of SWTBL interaction in the vicinity of a high speed vehicle [9]

Overview

The report is divided into six chapters. Chapter 2 presents an introduction to shock /turbulent boundary layer interaction. It also describes the inviscid flow over a compression corner. Chapter 3 describes the simulation methodology. It presents the introduction to the turbulent models used in the simulations. It also explains about the numerical method used and there advantages and drawbacks. In all the cases described in the report, the computational results are based on detailed grid convergence studies. The flow physics details are emphasized. The focus of the work is to predict the flow topology in the interaction region accurately. Specifically, the variation of temperature at respective position was studied. The potential and limitations of the effect of Reynolds number are assessed.

Shock/turbulent boundary layer interaction flows

The flow past a hypersonic vehicle is the seat of strong shock waves forming ahead of the vehicle nose, the rounded leading-edge of wings and tails, at the air-intake compression ramps of an air-breathing propulsion system, at the control surfaces, at the rear part of an after body where the nozzle jets meet the outer stream, to name the most salient examples.These shock waves are the main cause of heating and are at the origin of interferences resulting from their intersections and interactions with the boundary layer developing on the vehicle surface. Shock wave/boundary layer interactions (SWBLIs) can induce separation which causes loss of a control surface effectiveness, drop of an air intake efficiency and may be at the origin of large scale fluctuations such as air-intake buzz,buffeting or fluctuating side loads in separated propulsive nozzles. In high enthalpy flows,the subsequent reattachment on a nearby surface of the separated shear layer gives rise to local heat transfer rates which can be far in excess of those of an attached boundary layer.The large amount of experimental results on shock wave/boundary layer interaction in 2D flows has allowed a clear identification of the role played by the main parameters involved in the interaction process. Also correlation laws have been deduced giving the upstream interaction length, the limit for shock induced separation and, of prime importance in

ISSN No: 2348-4845
International Journal & Magazine of Engineering, Technology, Management and Research
A Peer Reviewed Open Access International Journal

hypersonic flows, the peak heat transfer at reattachment. Although the vast majority of configurations in the real world are three-dimensional, this report is focussed on the specific features of hypersonic SWBLIs in 2D and/or antisymmetric flows, which is sufficient to identify the influence of the key parameters involved in hypersonic interactions.

The consequences of high Mach number and enthalpy levels, typical of hypersonic flows, are multiple:

- Due to large differences in temperature within the flow field, adiabatic wall conditions are rarely reached, hence a specific effect of wall temperature.
- Because of the large temperature variation in the dissipative regions, density undergoes a large decrease in the boundary layer, hence an amplification of the displacement effect which, in conjunction with the pressure-deflection dependence, leads to strong viscous/inviscid coupling effects.
- The shock waves forming in the flow are very intense and interact strongly with the boundary layers giving rise to a further amplification of the viscous effects.
- In truly hyperenthalpic flows, the heating caused by shocks affects the gas thermodynamic properties, the resulting real gas effects influencing the interacting flow.
- The shock forming ahead of a hypersonic vehicle being both intense and highly curved, the vehicle is surrounded by a layer of rotational fluid or entropy layer which affects the boundary layer development and its further interaction with a shock wave.
- The conjunction of high Mach number and low density at high altitude tends to maintain a laminar regime over a great part of the vehicle surface. Thus, situations are encountered where SWBLIs are laminar or transitional, the pressure gradients associated with the interaction tending to precipitate the laminar-boundary layer transition.
- The strong coupling between the interaction and the flow inviscid part induces shock waves which interfere between them to generate complex shock patterns.

General considerations: The basic interactions

The three basic interactions between a shock wave and a boundary layer are the ramp flow,the impinging reflecting shock, and the pressure discontinuity resulting from adaptation to a higher downstream pressure level. The first case corresponds to a control surface or an air-intake compression ramp, the second to shock reflection inside an air intake of the mixed supersonic compression type, the third to the condition at the exit of an over expanded nozzle.

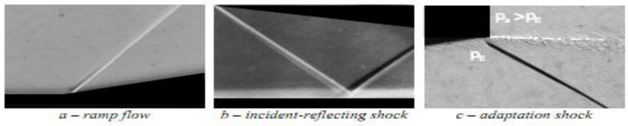

Figure: The three basic shock wave/boundary layer interactions

The compression ramp flow

When the ramp angle _ is small, the overall flow structure is not much affected by the interaction taking place at the ramp origin. The main difference is a spreading of the wall pressure distribution, the step of the inviscid solution being replaced by a progressive rise between the upstream level p0 and the final value p1 corresponding to the oblique shock equations. The spreading of the wall pressure distribution denotes the upstream influence mechanism through which the presence of the shock is felt upstream of its origin in perfect fluid; i.e., the ramp apex. As shown in , this upstream propagation results from the existence of a subsonic layer in the boundary layer inner part through which any signal (a pressure change) is propagated both in the upstream and downstream directions. The compression associated with the shock causes a progressive dilatation of the subsonic channel inducing in the supersonic contiguous part of the flow compression waves which coalesce to constitute the ramp induced shock at some distance from the wall. In a turbulent boundary layer, the subsonic channel is

ISSN No: 2348-4845
International Journal & Magazine of Engineering, Technology, Management and Research
A Peer Reviewed Open Access International Journal

extremely thin so that this shock forms within the boundary layer which behaves like an inviscid rotational fluid over most of its thickness.The interaction is said a rapid interaction process in which viscous forces play a negligible role compared to the action of pressure and momentum terms. However, because of the no-slip condition, to avoid inconsistencies a thin viscous layer in contact with the wallmust be considered.

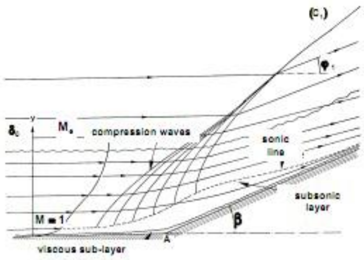

Figure: The structure of a ramp flow without boundar

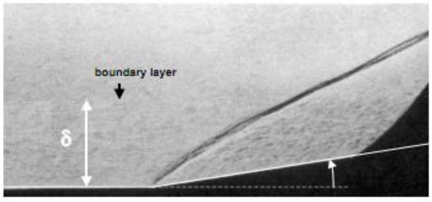

Figure: Turbulent ramp flow without separation at high Layer seperationMach and Reynolds numbers

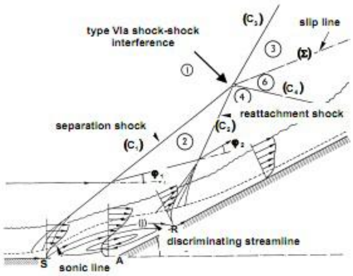

Figure: The structure of a ramp flow with boundary layer

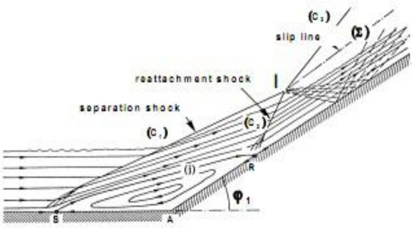

Figure: Ramp flow with boundary layer separation at high Mach

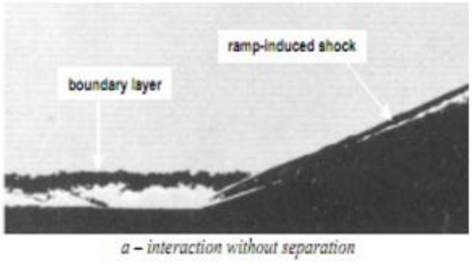

Separation number

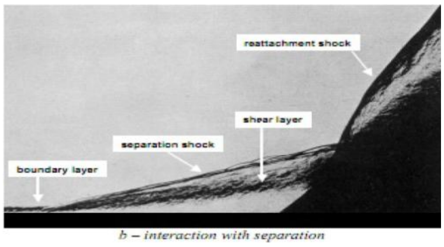

Effect of Reynolds number

As Mach number increases, the minimum of wall shear stress is decreased. It reaches zero at a point where a tiny separation bubble is formed (incipient separation). With further increase in Mach number, the separation bubble grows and the interaction becomes strong to very strong pattern.

Separation pressure rise, psinsensitive to variation of Reynolds number when Mach No. is relatively small. psdepends on Reynolds No. for higher Mach number. psis independent of Reynolds no. for minimum Mach no. necessary to separate the boundary layer.

Turbulent boundary layer separation pressure rise is nearly the same for both interactions of a compression ramp and an incident shock wave. Laminar boundary layer separation pressure rise is significantly small, compared with turbulent boundary layer.

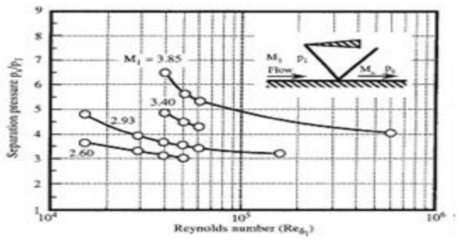

Figure: Effect of Reynolds number on SWTBL on flat on compression plate

ISSN No: 2348-4845
International Journal & Magazine of Engineering, Technology, Management and Research
A Peer Reviewed Open Access International Journal

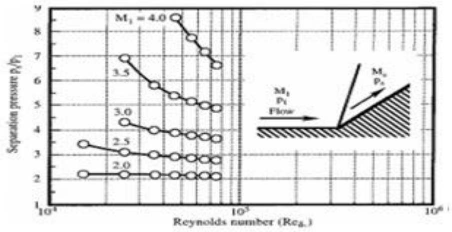

Figure 2.7: Effect of Reynolds number on SWTBL corner

Influence of wall temperature

The development of a boundary layer depends strongly on the thermal conditions at the wall, i.e. more precisely on the ratio of the wall temperature Tw to the adiabatic recovery temperature T . For example, an energetic cooling tends to postpone to higher Reynolds numbers laminar to turbulent transition and this has been considered as a means of reducing friction drag under some special circumstances. Furthermore, wall cooling has a favourable effect when applied in regions where the boundary layer is submitted to an adverse pressure gradient. Thus, separation can be prevented or largely postponed.

Such behaviour can be understood by considering the consequences of wall heat transfer on the development of a boundary layer. Let us recall that lowering the temperature of a gas reduces its molecular viscosity. Thus for the same development run, the profile of a cooled boundary layer will be fuller than that of an adiabatic boundary layer (the effect being like an increase in the local Reynolds number). More precisely, wall cooling (Tw=Ts<1) will produce the following changes with respect to the adiabatic case, at the same value of the Reynolds number R_ (only the turbulent case is considered)

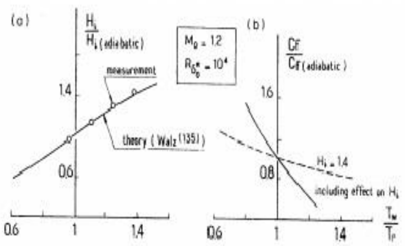

Figure: Wall temperature effect on some boundary layer properties

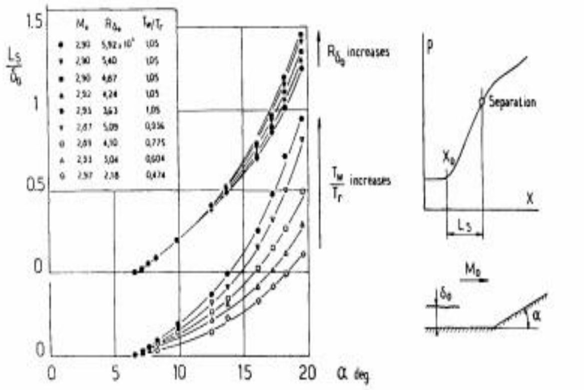

Figure: Supersonic interaction. Influence of Reynolds number and heat transfer at low to moderate Reynolds number

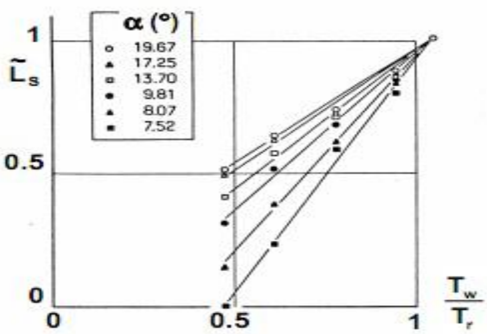

Figure: Supersonic interaction. Influence of heat transfer on the normalized separationlength

Thus, in the light of the results presented, it can already be anticipated that cooling of the wall will have favorable consequences on shock wave/boundary layer interactionsince it increases the stiffness of the dissipative flow. Moreover, the accompanying rise in wall shear stress will delay occurrence of separation by virtue of the mechanism revealed by the Free Interaction Theory. As we can see, wall cooling has a favourable effect via its action both on the viscous and inertia terms.

Simulation methodology

This describes the conservation equations and boundary conditions for two dimensional flow of a compressible fluid. This is followed by the numerical method for solving the governing equations.

ISSN No: 2348-4845
International Journal & Magazine of Engineering, Technology, Management and Research
A Peer Reviewed Open Access International Journal

Navier-Stokes equations

The instantaneous continuity, momentum and energy equations for compressible flows can be written in tensor notation as,

$$\frac{\partial}{\partial t}[\rho(e + 1/2 u_i u_i)] + \frac{\partial}{\partial x_j}[\rho u_j(h + 1/2 u_i u_i)] = \frac{\partial}{\partial x_j}(u_i t_{ij}) - \frac{\partial}{\partial x_j} q_j$$

$$t_{ij} = 2\mu s_{ij} - \zeta \frac{\partial u_k}{\partial x_k}\delta_{ij}$$

$$\mu = [\frac{(1.45 \times T^{6/2})}{(T + 110)} \times 10^{-6}]$$

$$q_j = -\kappa \frac{\partial T}{\partial x_j} = -\mu \times Pr_L \frac{\partial h}{\partial x_j}$$

$$p = \rho R T$$

$$e = C_v T$$

$$h = C_p T$$

Reynolds averaging

The Reynolds-averaged Navier-Stokes equations (or RANS equations) are time-averaged equations of motion for fluid flow. The idea behind the equations is Reynolds decomposition, whereby an instantaneous quantity is decomposed into its time-averaged and fluctuating quantities. The RANS equations are primarily used to describe turbulent flows.These equations can be used with approximations based on knowledge of the properties of flow turbulence to give approximate time-averaged solutions to the Navier-Stokes equations.

Adapted approaches in turbulence applied for incompressible flows is called Reynolds averaging and that which is applied for compressible flows is called Favre averaging. For statistically steady and stationary incompressible turbulence flow, the instantaneous variables are written as,

$$u_i(\vec{x}, t) = \overline{u}_i(\vec{x}) + u_i'(\vec{x}, t)$$

$$\overline{u}_i(\vec{x}) = \lim_{T\to\infty} \frac{1}{T}\int_t^{t+T} u_i(\vec{x}, t)dt$$

$$u_i = \overline{u}_i + u_i'$$

$$\rho = \overline{\rho} + \rho'$$

$$p = \overline{p} + p'$$

$$T = \overline{T} + T'$$

In Favre averaging the instantaneous variables are mass weighted averaged. For statistically steady and stationary compressible turbulence flow, the instantaneous variables are written as,

$$u_i(\vec{x}, t) = \tilde{u}_i(\vec{x}) + u_i''(\vec{x}, t)$$

$$\tilde{u}_i(\vec{x}) = \frac{1}{\overline{\rho}}\lim_{T\to\infty} \frac{1}{T}\int_t^{t+T} \rho(\vec{x}, t)u_i(\vec{x}, t)dt$$

$$u_i = \tilde{u}_i + u_i''$$

$$\rho = \overline{\rho} + \rho'$$

$$p = \overline{p} + p'$$

$$T = \tilde{T} + T''$$

$$e = \tilde{e} + e''$$

$$h = \tilde{h} + h''$$

The Favre average conservation law of mass, momentum and energy for steady, stationary and compressible turbulent flow can be derived by time averaging and are stated as,

$$\begin{aligned}
\frac{\partial \overline{\rho}}{\partial t} + \frac{\partial}{\partial x_i}(\overline{\rho}\tilde{u}_i) &= 0 \\
\frac{\partial}{\partial t}(\overline{\rho}\tilde{u}_i) + \frac{\partial}{\partial x_j}(\overline{\rho}\tilde{u}_i\tilde{u}_j) &= -\frac{\partial \overline{p}}{\partial x_i} + \frac{\partial(\overline{t}_{ij} - \tau_{ij})}{\partial x_j} \\
\frac{\partial}{\partial t}(\overline{\rho}\tilde{E}) + \frac{\partial}{\partial x_j}(\overline{\rho}\tilde{u}_j\tilde{H}) &= -\frac{\partial}{\partial x_j}(q_{L_j}) - \frac{\partial}{\partial x_j}(q_{T_j}) + \frac{\partial}{\partial x_j}(\tilde{u}_i\overline{t}_{ij}) + \frac{\partial}{\partial x_j}(\tilde{u}_i\tau_{ij} \\
&\quad - \frac{\partial}{\partial x_j}\overline{\rho u_i'' u_i'' u_j''} + \frac{\partial}{\partial x_j}\overline{(t_{ij}u_i'')}
\end{aligned}$$

$$\tilde{E} = \tilde{e} + \frac{1}{2}\tilde{u}_i\tilde{u}_i + k$$

$$\tilde{H} = \tilde{h} + \frac{1}{2}\tilde{u}_i\tilde{u}_i + k$$

$$\tilde{e} = C_v\tilde{T}$$

$$\tilde{h} = \tilde{e} + \overline{p}/\overline{\rho}$$

where, $$k = \frac{1}{2}\frac{\overline{\rho u_i'' u_i''}}{\overline{\rho}}$$

$$\overline{t}_{ij} = 2\mu(S_{ij} - \frac{1}{3}S_{kk}\delta_{ij})$$

$$\tau_{ij} = -\overline{\rho u_i'' u_j''}$$

The first and second terms on RHS of Eq. 3.16 represent the conduction heat flux and turbulent heat flux. The conduction heat flux is calculated from Fourier's assumption of heat conduction which is given as

$$q_{L_j} = -\frac{\mu}{Pr_L}\frac{\partial \tilde{h}}{\partial x_j} = -\frac{\mu C_p}{Pr_L}\frac{\partial \tilde{T}}{\partial x_j} = -\kappa\frac{\partial \tilde{T}}{\partial x_j}$$

and the turbulent heat flux vector is defined as,

$$q_{T_j} = \overline{\rho u_j'' h''}$$

In terms of mean variables the equation of state for perfect gas is expressed as,

$$\overline{p} = \overline{\rho}R\tilde{T}$$

Spalart-Allmaras model

In one equation Spalart-Allmaras or SA Model [13] the eddy viscosity ν_T is related to the intermediate variable, $\tilde{\nu}$ by a damping function, f_{v1} as $\nu_T = \tilde{\nu} f_{v1}$, and the equation for $\tilde{\nu}$ is written as,

$$\frac{\partial \overline{\rho}\tilde{\nu}}{\partial t} + \frac{\partial \overline{\rho}\tilde{\nu}\tilde{u}_j}{\partial x_j} = c_{b1}\overline{\rho}\tilde{S}\tilde{\nu} - c_w f_w \overline{\rho}\left(\frac{\tilde{\nu}}{d}\right)^2 + \frac{1}{\sigma}\frac{\partial}{\partial x_k}\left[(\mu + \overline{\rho}\tilde{\nu})\frac{\partial \tilde{\nu}}{\partial x_k}\right] + \frac{c_{b2}\overline{\rho}}{\sigma}\frac{\partial \tilde{\nu}}{\partial x_k}\frac{\partial \tilde{\nu}}{\partial x_k}$$

In shorthand this is written as,

$$\frac{D\overline{\rho}\tilde{\nu}}{Dt} = \mathrm{Prod}(\tilde{\mathrm{S}}, \overline{\rho}\tilde{\nu}, \mathrm{d}) - \mathrm{Dest}(\overline{\rho}\tilde{\nu}, \mathrm{d}) + \frac{1}{\sigma}[\nabla.((\mu + \overline{\rho}\tilde{\nu})\nabla\tilde{\nu}) + c_{b2}\overline{\rho}(\nabla\tilde{\nu})^2]$$

Here,

$$f_w = g\left[\frac{1 + c_{w3}^6}{g^6 + c_{w3}^6}\right], \qquad f_{v1} = 1 - \left[\frac{\chi^3}{\chi^3 + c_{v1}^3}\right], \qquad f_{v2} = 1 - \frac{\chi}{1 + \chi f_{v1}}$$

where,

$$\chi = \frac{\tilde{\nu}}{\nu}, \qquad g = r + c_{w2}(r^6 - r), \qquad r = \frac{\tilde{\nu}}{\tilde{S}\kappa^2 d^2}, \qquad \tilde{S} = S + \frac{\tilde{\nu}}{\kappa^2 d^2} f_{v2}$$

d is the normal distance from the wall and the vorticity magnitude is represented as $\overline{S} = \sqrt{(2\Omega_{ij}\Omega_{ij})}$, in which the rotation tensor is given as $\Omega_{ij} = \frac{1}{2}[(\frac{\partial \tilde{u}_i}{\partial x_i}) - (\frac{\partial \tilde{u}_j}{\partial x_j})]$ and the constants are given as $c_{b1} = 0.1355, c_{b2} = 0.622, c_{v1} = 7.1, \sigma = 2/3, \kappa = 0.41, c_{w1} = c_{b1}/\kappa^2 + (1 + c_{b2})/\sigma, c_{w2} = 0.3, c_{w3} = 2.$

The terms on the LHS of Eq. 3.35 represent the transport terms. The first and second terms on RHS of Eq. 3.35 represent the production and destruction of eddy viscosity. The last two terms on RHS represent the molecular and eddy diffusivity terms. The quantities embraced within them represents the major variables dependency of these source terms.

Boundary-conditions for turbulence models

The free stream and wall boundary conditions for various turbulence models are stated below with subscript ∞ and w representing the free stream and wall conditions.

$$\tilde{\nu}_\infty = \frac{0.1\mu_\infty}{\overline{\rho}_\infty} \text{ and } (\nu_{T_w}) = 0$$

The free stream and wall boundary conditions for various turbulence models are stated below with subscript ∞ and w representing the free stream and wall conditions.

$$\tilde{\nu}_\infty = \frac{0.1\mu_\infty}{\overline{\rho}_\infty} \text{ and } (\nu_{T_w}) = 0$$

Generic form of governing equation

In this section we use standard one-equation Spalart-Allmaras model to calculate the eddy viscosity. In two-dimensional RANS equations we solve for one continuity, two momentum, one energy and one transport equation of viscosity equation along with turbulent closure equations.

$$\frac{\partial U}{\partial t} + \nabla.(\vec{F} + \vec{G}) = Q$$

$$\frac{\partial U}{\partial t} + \frac{\partial F}{\partial x} + \frac{\partial G}{\partial y} = Q$$

$$F = F_I + F_V; \qquad G = G_I + G_V$$

$$U = [\overline{\rho} \quad \overline{\rho}\tilde{u} \quad \overline{\rho}\tilde{v} \quad \overline{\rho}\tilde{E} \quad \overline{\rho}\tilde{\nu}]^T$$

$$F_I = \begin{bmatrix} \overline{\rho}\tilde{u} \\ \overline{\rho}\tilde{u}^2 + \overline{p} + \frac{2}{3}\overline{\rho}k \\ \overline{\rho}\tilde{u}\tilde{v} \\ (\overline{\rho}\tilde{E} + \overline{p} + \frac{2}{3}\overline{\rho}k)\tilde{u} \\ \overline{\rho}\tilde{\nu}\tilde{u} \end{bmatrix}; \qquad G_I = \begin{bmatrix} \overline{\rho}\tilde{v} \\ \overline{\rho}\tilde{u}\tilde{v} \\ \overline{\rho}\tilde{v}^2 + \overline{p} + \frac{2}{3}\overline{\rho}k \\ (\overline{\rho}\tilde{E} + \overline{p} + \frac{2}{3}\overline{\rho}k)\tilde{v} \\ \overline{\rho}\tilde{\nu}\tilde{v} \end{bmatrix}$$

$$F_V = \begin{bmatrix} 0 \\ \overline{t}_{xx} + \tau_{xx} \\ \overline{t}_{xy} + \tau_{xy} \\ (\overline{t}_{xx} + \tau_{xx})\tilde{u} + (\overline{t}_{xy} + \tau_{xy})\tilde{v} + (\kappa + \kappa_T)\frac{\partial \tilde{T}}{\partial x} + (\overline{\mu} + \sigma\mu_T)\frac{\partial k}{\partial x} \\ (\frac{1}{\sigma}[(\mu + \overline{\rho}\tilde{\nu})] + \frac{c_{b2}\overline{\rho}}{\sigma}\tilde{\nu})\frac{\partial \tilde{\nu}}{\partial x} \end{bmatrix}$$

$$G_V = \begin{bmatrix} 0 \\ \overline{t}_{xy} + \tau_{xy} \\ \overline{t}_{yy} + \tau_{yy} \\ (\overline{t}_{xy} + \tau_{xy})\tilde{u} + (\overline{t}_{yy} + \tau_{yy})\tilde{v} + (\kappa + \kappa_T)\frac{\partial \tilde{T}}{\partial y} + (\overline{\mu} + \sigma\mu_T)\frac{\partial k}{\partial y} \\ (\frac{1}{\sigma}[(\mu + \overline{\rho}\tilde{\nu})] + \frac{c_{b2}\overline{\rho}}{\sigma}\tilde{\nu})\frac{\partial \tilde{\nu}}{\partial y} \end{bmatrix}$$

Finite volume method

The governing equations of fluid dynamics can be expressed in differential form. Numerical scheme is applied to these equations to divide the domain into gird points and finite difference equations are solved. Alternate approach is to solve the integral form. In this approach the physical domain is divided to small areas(areas in 2-D case). Dependent variables are evaluated either at the centres of the volume or at the corners of the volumes.

In order to explain finite volume method consider 2-d model equation

$$\frac{\partial U}{\partial t} + \frac{\partial F}{\partial x} + \frac{\partial G}{\partial y} = 0$$

Integrating over finite volume abcd (unit depth) gives

$$\int\int\int_{abcd}(\frac{\partial U}{\partial t} + \frac{\partial F}{\partial x} + \frac{\partial G}{\partial y})\mathrm{d}\,v = 0$$

$$\frac{\partial}{\partial t}\int\int\int_{abcd} U(1)\,\mathrm{d}\,x\,y + \oint\oint H.n\,\mathrm{d}\,S = 0$$

Where n is unit vector normal surface S of the control volume. H can be expressed as

$$H.n\,\mathrm{d}\,S = (E\,\mathrm{d}\,y - F\,\mathrm{d}\,x)(1)$$

The solution can be solved to

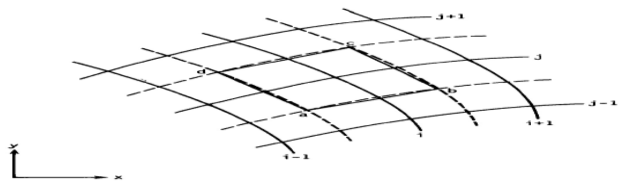

Figure: Two Dimensional Finite Volume

$$\frac{\partial}{\partial t}\int\int_{abcd} U(1)\,\mathrm{d}\,x\,y + \oint_{abcd}(E\,\mathrm{d}\,y - F\,\mathrm{d}\,x) = 0$$

This can be approximated to

$$\frac{(U_{i,j}^{n+1} - U_{i,j}^n)}{t}S_{abcd} + (E_{i,j-1/2}\triangle y_{ab} + E_{i-1/2,j}\triangle y_{bc} + E_{i,j+1/2}\triangle y_{cd} + E_{i+1/2,j}\triangle y_{da})$$
$$-(F_{i,j-1/2}\triangle x_{ab} + F_{i-1/2,j}\triangle x_{bc} + F_{i,j+1/2}\triangle x_{cd} + F_{i+1/2,j}\triangle x_{da}) = 0$$

$$\frac{\partial}{\partial t}\iiint_{CV} U dV + \iint_{CS}[(\vec{F_I} + \vec{G_I}) + (\vec{F_V} + \vec{G_V})].(\hat{\jmath}n dS) = \iiint_{CV} Q dV$$

$$\frac{\partial U}{\partial t} = -\frac{1}{V_{i,j}}\left[\vec{F}_{i+1/2,j}.\vec{S}_{i+1/2,j} + \vec{F}_{i-1/2,j}.\vec{S}_{i-1/2,j} + \vec{G}_{i,j+1/2}.\vec{S}_{i,j+1/2} + \vec{G}_{i,j-1/2}.\vec{S}_{i,j-1/2}\right] + Q$$

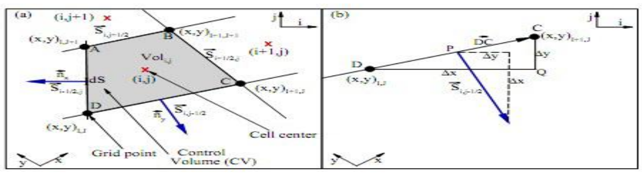

$$\vec{S}_{i+1/2,j} = +(y_{i+1,j+1} - y_{i+1,j})\hat{\imath} - (x_{i+1,j+1} - x_{i+1,j})\hat{\jmath}$$
$$\vec{S}_{i-1/2,j} = -(y_{i,j+1} - y_{i,j})\hat{\imath} + (x_{i,j+1} - x_{i,j})\hat{\jmath}$$

$$V_{i,j} = [|(x_{i,j} - x_{i+1,j})y_{i+1,j+1} + (x_{i+1,j} - x_{i+1,j+1})y_{i,j} + (x_{i+1,j} - x_{i,j})y_{i+1,j}|$$
$$+|(x_{i,j} - x_{i+1,j+1})y_{i,j+1} + (x_{i+1,j+1} - x_{i,j+1})y_{i,j} + (x_{i,j+1} - x_{i,j})y_{i+1,j+1}|]$$

$\hat{n}$ is the unit normal vector to surface area dS as shown in Fig. 3.2. Here $\vec{S}_{i+1/2,j}$ and $S_{i-1/2,j}$ are the surface area vectors and,$\hat{i}$ and $\hat{j}$ are unit vectors in i and j direction. x and

ISSN No: 2348-4845
International Journal & Magazine of Engineering, Technology, Management and Research
A Peer Reviewed Open Access International Journal

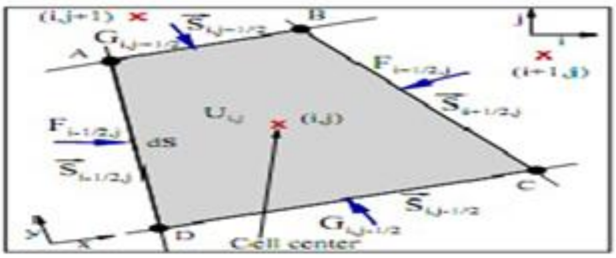

Figure 3.3: The conservative variable $U_{I,J}$ at cell center calculated from the fluxes F and G passing through the cell boundaries in the x- and y-directions. [14]

Summary

Reynolds-averaged Navier-Stokes equations are described for simulation of high-speedflows. Commonly used one- and two-equation turbulence models are used for turbulenceclosure. They provide a trade-off between computational efficiency and accuracy of thesolution. A finite volume based numerical method is described. It uses modified Roe fluxdifference splitting approach for computing the inviscid fluxes, and second-order centraldifference for the viscous fluxes and turbulent source terms.

Inviscid simulation over compressioncorner

Introduction

In this chapter the flow over a compression corner of _ = 28_ is studies at Mach 5. Theoccurrence of supersonic / hypersonic flow over compression corner can be found onmany practical high-speed flow applications, to name a few, the control surfaces (such aselevators, wing- and body-flaps) and air intake compression ramps of the air-breathingpropulsion system on re-entry vehicles as well as high-speed aircraft. The dramaticsignificance of such phenomenon in application have induced much attention from manyresearchers, hence lots of related studies, either experimentally or numerically, have beenconducted extensively over the past few decades.

As the high-speed flow pass through the compression corner, it would first experience compressive disturbance and subsequently its streamline is deflected, accompanying bythe formation of oblique shock wave. The development of shock wave can be elucidatedas followed; the disturbance waves caused by the corner would try to propagate withsonic speed to surrounding regions, including directly upstream, for communicating thechanges of energy and momentum to other regions of the flow. Nevertheless, since theincoming mainstream is supersonic/hypersonic, the disturbance waves could no longertravel upstream. Instead, they would coalesce a short distance ahead of the corner into athin layer which is in fact the shock wave itself. This case is particularly true for inviscid flow, where the pressure of the flow increases discontinuously across the shock wave.

The experimental data test conditions are listed below.

Free stream Mach number M_∞	4.95
Stagnation temperature T_0	359 K
Static temperature T_∞	59.3
Stagnation pressure P_0	2.28 MPa
Static pressure P_∞	4348.59 Pa
Unit Reynolds number $Re_{1\infty}$	$49.9 \times 10^6 m^{-1}$
Density ρ_∞	1.125

Free stream conditions of shock-wave turbulent boundary-layer interaction overcompression corner.

Simulation over compression corner at Mach 5 with $\theta = 28°$

The flow for inviscid case is first studied and verified with inviscid theory.

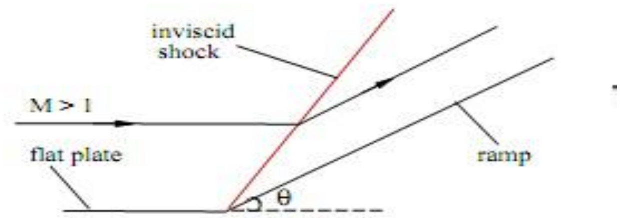

Fig :Inviscid supersonic flow over compression corner generating an oblique shock at the corner

Computational grid

The grid generation for the present case is shown in Fig. 4.2. A uniform gird has beenused with 400 cells along i-direction and 200 cells along j-direction. The physical planeadopts a Cartesian coordinate system. The surface including the compression corner formsthe lower boundary in this physical plane. The inflow

ISSN No: 2348-4845
International Journal & Magazine of Engineering, Technology, Management and Research
A Peer Reviewed Open Access International Journal

boundary is placed at x = 0 and theoutflow boundary is at x = L.

Pressure far field boundary condition is applied to inflow and the top surface as it issuitable for compressible flows. Wall condition is not taken for the top surface as in caseof strong shock formation intersection with wall will result in shock reflection and shock interaction, which is undesired. The Wall is taken as adiabatic for this case.

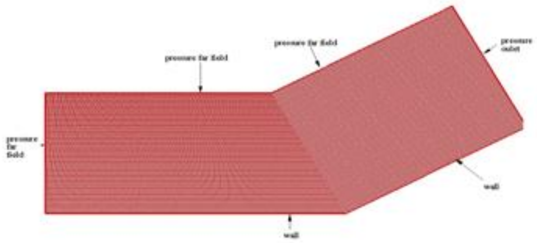

Fig: Grid for inviscid supersonic flow over compression corner

Simulation Result

Figures shows the Mach number contour plot for the inviscid supersonic flow over thecompression corner. Notice that there is oblique shock exists on the ramp and an abruptchange in flow velocity occurs across the shock. When the flow past over the compressioncorner, the flow streamline would be deflected upward, through the main bulk of the flowabove the surface. This introduces compressive disturbance onto the flow. The disturbancesignals would attempt to travel with sonic speed to the surrounding regions (upstream anddownstream) to communicate the changes of momentum and energy to the nearby region.However, due to the supersonic flow of the free stream, this disturbance signals is unableto travel upstream. Rather, they would be carried downstream and form a thin layer at ashort distance ahead of the corner which could be visualized as the shock wave.

The below table shows the computed, theoretical and percentage error. The erroris due to the discritization of the domain. The error can be reduced by grid refinement.

The reason for CFD error are, for the most part, dependent upon the concept ofnumerical errors that are generated throughout the course of a given calculation and, moreto the point, the way that these errors are propagated from one marching step to the next.Simply stated, if a given numerical error is amplified in going from one step to the next,then the calculation will become unstable; if the error does not grow, and especially if itdecreases from one step to another, then the calculation usually has a stable behaviour.Therefore, a consideration of stability must first be prefaced by a discussion on numericalerrors--what they are and what they are like.

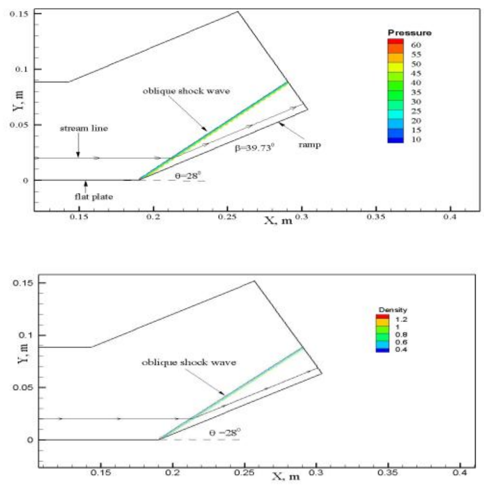

Fig: Computed (a) pressure and (b) density contours for flow over compression corner

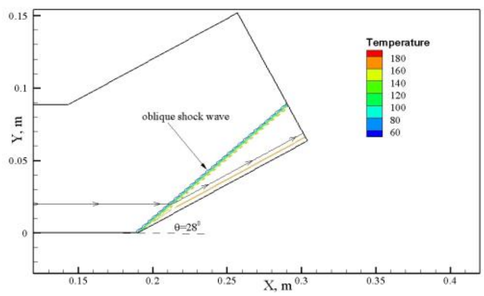

ISSN No: 2348-4845
International Journal & Magazine of Engineering, Technology, Management and Research
A Peer Reviewed Open Access International Journal

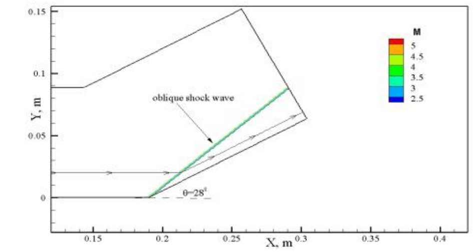

Fig: Computed (a) temperature and (b) mach number contours for flow overcompression corner

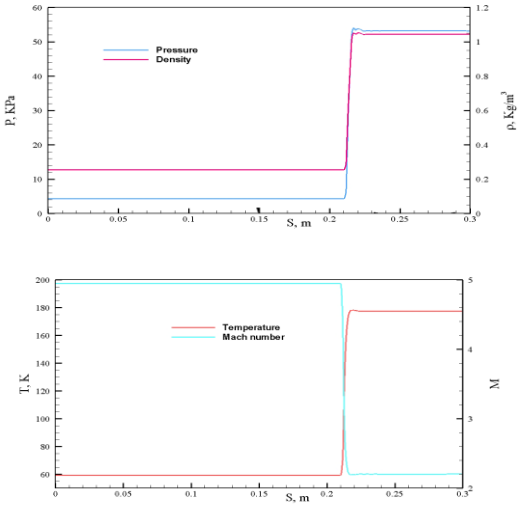

Figure 4.5: (a) pressure , density (b) temperature and mach number change across a shock wave

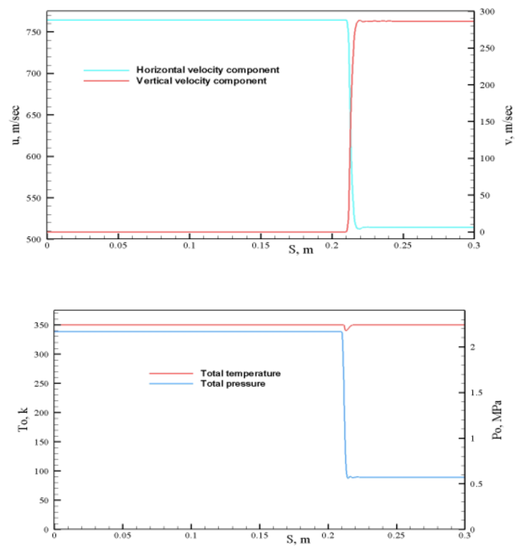

Fig: (a) Horizontal velocity , vertical velocity (b) total pressure variation across a shock wave

Parameters	CFD	Inviscid theory	error
P_2/P_1	11.98	11.51	4.14
T_2/T_1	3.01	2.87	5.37
M_2/M_1	0.44	0.46	4.45
ρ_2/ρ_1	4.01	4.00	0.128
u_2/V_1	0.6704	0.659	1.700
v_2/V_1	0.376	0.369	1.68

Table: Comparison of simulated results with inviscid results

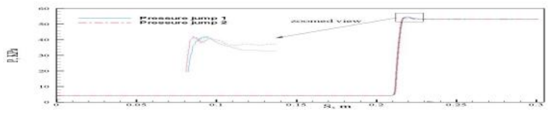

Fig: Pressure profile for first and second order for inviscid case at corner angle 28degree

CFD error

Discretization error, the difference between the exact analytical solution of the partialdifferential equation and the exact (round-off-free) solution of the corresponding difference equation. .From our discussion , the discretization error is simply the truncation errorfor the difference equation plus any errors introduced by the numerical treatment of theboundary conditions. It results in dissipation, smoothing of the solution occurs.Round-off error, the numerical error introduced after a repetitive number of calculationsin which the computer is constantly rounding the numbers to some significant figure.This results in dispersion error, oscillation of the solution, as the order increases dispersiondominates dissipation. Thus dissipation occurs in lower order and dispersion occurs inhigher order schemes.

Oblique shock-wave / turbulentboundary-layer interaction

Oblique shock wave simulation

The flow taking viscosity into consideration has been simulated. The length of the plate isincreased compared to viscid case so as to obtain undisturbed turbulent boundary-layerproperties.

Computationalgrid

The gird generated for the present case is as shown in Fig.To complete capture theboundary layer and recirculation bubble properties exponential stretching

ISSN No: 2348-4845
International Journal & Magazine of Engineering, Technology, Management and Research
A Peer Reviewed Open Access International Journal

of the grid hasbeen done along i and j directions. A minimum cell size of 1_10-6m is taken in the i

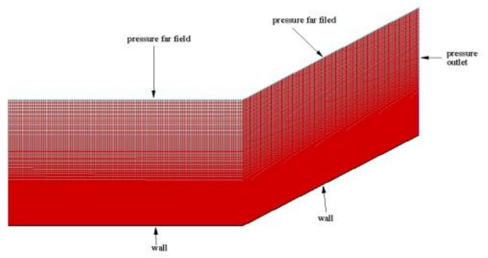

Fig : Grid for supersonic flow over compression corner

direction (normal direction of wall) and 1 _ 10□3 in taken in the j direction. The totalnumber cells is given as 1000 _ 400.

The boundary conditions isas shown in Fig.The region at the top, where extrapolationcondition is used to avoid reflection of shock waves. At the wall adiabatic, no-slip andzero pressure gradient boundary conditions are assigned.

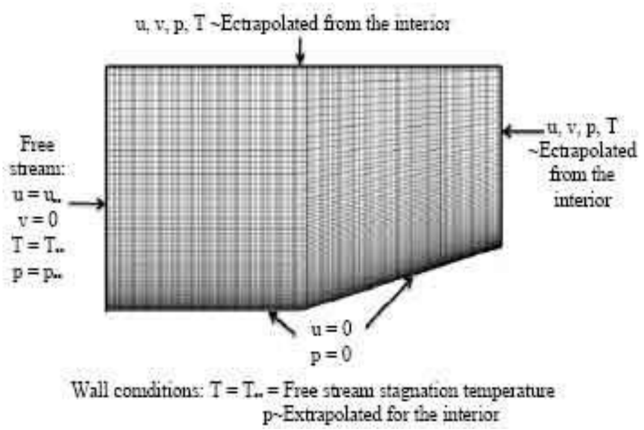

Fig: Boundary conditions of the domain

Simulation result

The flow field characteristic of the turbulent supersonic flow over compression cornershowing has been investigated.

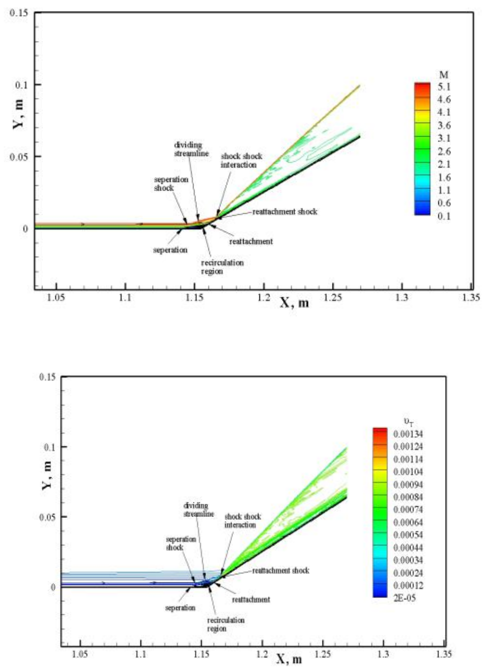

Fig :Turbulent supersonic flow over compression corner showing, (a) Machnumber and (b) eddy viscosity contours for adiabatic wall with unit

Reynolds number $Re_{1\infty}$ $78.6 \times 10^{6} \mathrm{m}^{-1}$
Observations made

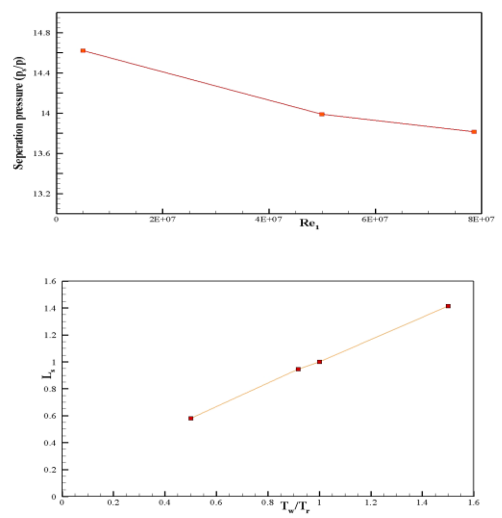

Fig :Effect of Reynolds number on separation pressureFig : Effect of temperature of shock bubble length

ISSN No: 2348-4845
International Journal & Magazine of Engineering, Technology, Management and Research
A Peer Reviewed Open Access International Journal

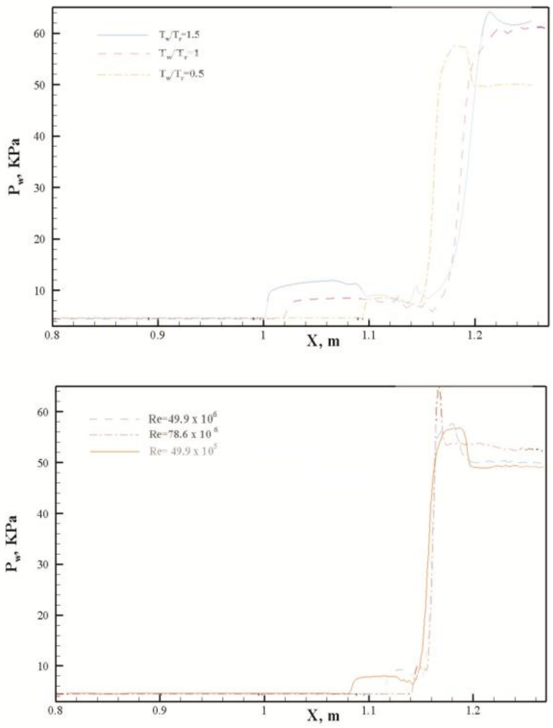

Fig: (a) Wall temperature and (b) Reynolds number effect on wall pressure

Conclusion

This work had investigated the supersonic flow over 2-dimensional compression cornerfor both inviscid and turbulent case. Analysis was conducted for the corner angle 28 degreeat free stream velocity of Mach 5. The wall temperature and Reynolds number has beenvaried . Several conclusions can be drawn from the study:

- As the free stream density increases , the peak pressure decreases, separation tends tooccur and the recirculation region becomes more obvious and recirculation region length tend to decrease.
- As the wall temperature increases, there is increase in L . Lowering of the wall temperature provokes an increase of the skin friction coefficient and a reduction ofthe boundary layer displacement thickness (due to an increase of density) hence a increase of L.

The ramp angle can be changed and solved using different schemes. Besides, the problemcan also be extended into the case of hypersonic turbulent flow over compression cornerto explore the difference between the supersonic and hypersonic case.

References

1. Daniel Arnal and Jean Delery: Shock Wave Boundary Layer Interaction, NATO,May 2004.

2. Elfstrom, G.M. Turbulent hypersonic flow at a wedge compression corner. J. FluidMech., Vol. 53, Part 1, pp. 113-129, 1972.

3. Settles, G.S.: An experimental study of compressible boundary layer separation athigh Reynolds number. Ph. D. Thesis, Princeton University, 1975.

4. Walz. A. (1969) Boundary-Layers of Flow and Temperature, p. 113. M. I. T. Press.Cambridge. Mass.

5. Padova. C.. Falk. T. J. and Wittliff. C. E. (19801 Experimental investigation ofsimilitude parameters governing transonic shock/boundary-layer interactions. AIAAPaper No. 80-0158.

6. Inger, G. R. (1979)Transonic shock/boundary-layer interactions in cryogenic windtunnels, J. Aircr. 16(4), 284 287.

7. Frishett, J. C. (19711 Incipient separation of a supersonic turbulent boundary-layer including effects of heat transfer, Ph.D Dissertation, Univ. of California, Los Angeles

8. Spaid, F. W. and Frishett, J. C. (1972) Incipient separation of a supersonic, turbulentboundary-layer, including effects of heat transfer, AIAA J. 10(7), 915 922.

9. HolgerBabinsky, John K. Harvey(2011) Shock Wave-Boundary-Layer Interactions,p.138. Cambridge University Press.

10. Kim H. D. and Setoguchi. T. : Shock Induced Boundary Layer Separation, ISAIF,Lyon, France, July-2007.

11. Shames, E., Mechanics of Fluid Flow, McGraw-Hill, Inc., 4th ed., 2003.

12. Wilcox, D. C., Turbulence Modeling for CFD, DCW Industries, 2nd ed., 2000, pp.491-492.

13. Spalart, P. R., and Allmaras, S. R., A One-equation Turbulence Model for AerodynamicFlows, AIAA Paper 1992-0439, Jan. 1992.

14. Amjad Ali Pasha: Application of shock-unsteadiness model to hypersonic shock/turbulent boundary-layer interaction. Ph. D. Thesis, I. I. T. Bombay, 2012.

15. John C. Tannehill, Dale A. Anderson and Richard H. Pletcher (1984) Computationalfluid mechanics and heat transfer, Taylor and Francis.